CONTROL ANALYSIS OF FLEXIBLE SOLAR SAILS

Stephanie J. Thomas[1] and Michael A. Paluszek[2]

[1]*Senior Technical Staff, Princeton Satellite Systems, 33 Witherspoon St., Princeton, NJ, 08542, USA, Email: sjthomas@psatellite.com*

[2]*President, Princeton Satellite Systems, Email: map@psatellite.com*

ABSTRACT

Future solar sail missions will require sails with dimensions on the order of 100 m to 1 km. At these sizes, given the gossamer nature of the sail supporting structures, flexible modes may be low enough to interact with the control system. This paper develops a practical analysis of the flexible interactions using state-space systems and modal data from standard finite element models of the sail subsystem. The modal data is combined with a rigid core bus to create a modal coordinate state-space plant, which can be analyzed for stability with a state-space controller. Results are presented for an 80 m sail for both collocated actuation and control by actuators mounted at the sail tips.

1. INTRODUCTION

Future solar sail missions, such as NASA's Solar Polar Imager, will require sails with dimensions on the order of 100 m to 1 km. At these sizes, given the gossamer nature of the sail supporting structures, flexible modes may be low enough to interact with the control system. This paper develops a practical analysis of the flexible interactions using state-space systems and modal data from finite element models of the sail. The tools, part of the MATLAB^{TM}-based Solar Sail Module for the Spacecraft Control Toolbox developed under the NASA In-Space Propulsion program, include a graphical user interface which allows users to quickly perform analyses (Thomas et al. 2004).

Standard finite-element models of the flexible sail body are loaded and the modal data is used to create a modal coordinate state-space system. The analyst specifies which modes to include, which nodes are of interest for force inputs and displacement outputs, any nominal momentum in the system, and any steady rates. The system is linearized about the nominal attitude and body rates. The state-space plant can then be analyzed with a state-space controller, and Bode, Nyquist, step and impulse responses generated. The approach is general for any rigid core with a flexible appendage.

The sail analyzed is a square sail with four gossamer masts and four triangular sail membranes suspended between them. The coordinate frame of the sail - shown in a sun-synchronous Earth orbit - is given in Figure 1.

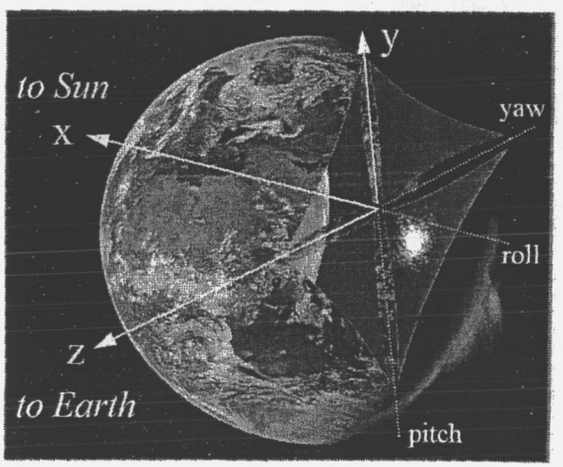

Figure 1. Sail Coordinate System (ATK Space Systems)

A finite element model of the scalable sail has been provided for this analysis by ATK Space Systems (Goleta, CA) (Murphy et al. 2005). The first 30 modes range from about 0.04 to 0.08 Hz. The model and modes can be effectively visualized in MATLAB as seen in Figure 2 on the next page. One control method under consideration is a suite of pulsed plasma thrusters mounted at the tip of the masts (Wie et al. 2004). On the $+Y$ axis for this model, the corresponding node at which the force will be applied is 50041. A $+X$ force applied here will produce a negative rotation about the Z axis.

This paper presents results for an 80 m sail controlled by a PID, such as would be implemented by reaction wheels or control moment gyros (CMGs) on the core bus. In addition the response to actuators mounted on the sail tips is

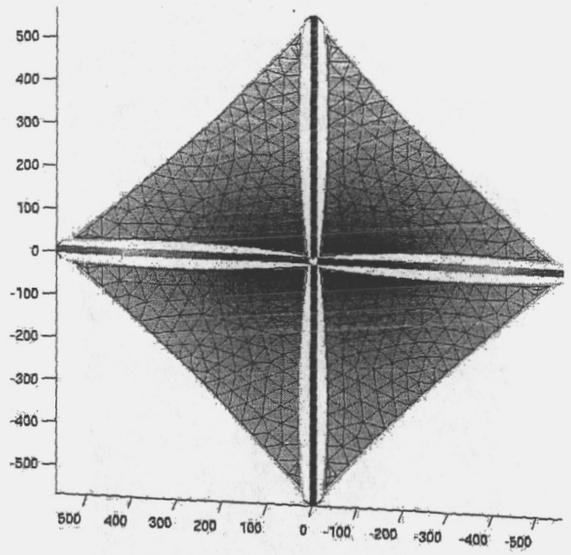

Figure 2. Solar sail mode visualization in MATLAB

shown, such as by control vanes or small thrusters. Both the overall control stability and the resulting deflection of any node is obtained.

2. DERIVATION OF LINEAR PLANT MODEL

We require a state-space form of the dynamics, i.e.

$$\begin{aligned} \dot{x} &= Ax + Bu \\ y &= Cx \end{aligned}$$

where x is the state, u is the control input, and y is the measured output.

Our vehicle consists of a rigid core and a flexible appendage. We begin by defining a set of nodes on the appendage. If the vector from system center of mass (C_{sys}) to the origin is c, the nominal node locations are r_k, and the nodal displacements are ρ_k, then the vectors from C_{sys} to the nodes are $d_k = c + r_k + \rho_k$. This is depicted in Figure 3.

We also define the modal displacements η, where the transformation matrix Φ gives the nodal displacement per unit modal displacement for each mode. Φ is constructed as a $3n \times m$ matrix, where n is the number of nodes and m is the number of modes. This can be written compactly in matrix notation as

$$\rho = \Phi\eta \tag{1}$$

Our goal is to develop state-space equations using the modal coordinates η. We begin with the total angular momentum of a rigid core with a flexible body about the spacecraft center-of-mass. Note that the sum includes the

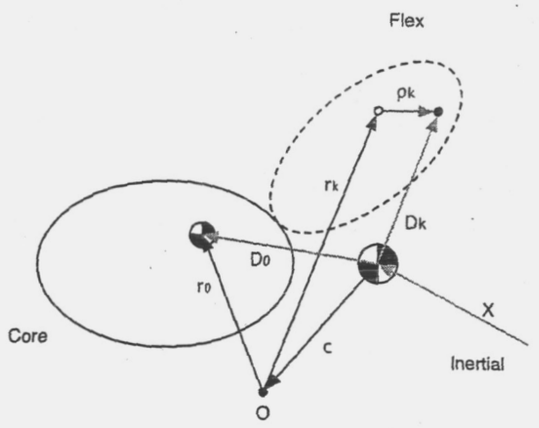

Figure 3. Node vector definitions

displacement of the core from the system center of mass as the sum starts at 0.

$$H = A(I\omega) + \sum_{k=0}^{n} m_k D_k^{\times} \dot{D}_k \tag{2}$$

where A is the rotation from the body frame to the inertial frame, I is the inertia matrix of the core and $D_k = Ad_k$ are the node vectors from the system center of mass in the inertial frame. Taking the inertial derivative and transforming to the body frame we have

$$T = I\dot{\omega} + \omega^{\times} I\omega + \sum_{k=0}^{n} m_k d_k^{\times} \ddot{d}_k \tag{3}$$

where T is the external torque on the spacecraft.

The second key equation is the inertial equation of motion for the nodal masses, including the motion of the spacecraft center-of-mass, $\ddot{X}$, produced by the total external force.

$$f_k = m_k(\ddot{d}_k + \ddot{X}) \tag{4}$$

where f_k is the sum of the internal forces exerted by adjacent nodes and any external forces on the nodes and $\ddot{X} = \sum F / \sum m$.

We manipulate this second equation first. The definition and derivatives of d are

$$\begin{aligned} d &= r + c + \rho \\ \dot{d} &= \omega^{\times} d + \dot{\rho} + \dot{c} \\ \ddot{d} &= \omega^{\times}\omega^{\times} d + \dot{\omega}^{\times} d + 2\omega^{\times}(\dot{\rho} + \dot{c}) + \ddot{\rho} + \ddot{c} \end{aligned}$$

where c, taking the origin O at the core center so that r_0 is zero, is

$$c = -\sum_{k=1}^{n} \frac{m_k(r_k + \rho_k)}{m_T} \tag{5}$$

Substituting this into Equation 4, dropping the nonlinear terms in ω, $\dot{\rho}$ and $\dot{c}$,

$$f_k \approx m_k(-d_k^{\times}\dot{\omega} + \ddot{\rho}_k + \ddot{c} + \frac{\sum F}{\sum m}) \tag{6}$$

The internal mass forces can also be represented as a spring force, giving

$$f_k \equiv -\sum_j k_{kj}(\rho_j - \rho_k) + F_k = -K\rho + F_k \tag{7}$$

where k is a physical property of the structure and F_k is the external force on each node.

Substituting the definitions of f_k and c we have

$$m_k(\ddot{\rho}_k + \ddot{c}) + K\rho = -m_k(-d_k^{\times}\dot{\omega} + \frac{\sum F}{\sum m}) + F_k \tag{8}$$

$$\begin{aligned} -m_k\frac{\sum F}{\sum m} + F_k &= \frac{m_T - m_k}{m_T}F_k - m_k\sum_{j\neq k}\frac{F_j}{m_T} \\ &= \nu_k F_k - \mu_k\sum F_j \end{aligned}$$

$$\begin{aligned} \ddot{\rho}_k + \ddot{c} &= \ddot{\rho}_k - \sum\frac{m_j\ddot{\rho}_j}{m_T} \\ &= \frac{m_T - m_k}{m_T}\ddot{\rho}_k - \sum_{j\neq k}\frac{m_j\ddot{\rho}_j}{m_T} \\ &= \nu_k\ddot{\rho}_k - \sum\mu_j\ddot{\rho}_j \end{aligned}$$

$$\begin{aligned} m_k(\nu_k\ddot{\rho}_k - \sum\mu_j\ddot{\rho}_j) + K\rho = \\ m_k d_k^{\times}\dot{\omega} + \nu_k F_k - \mu_k\sum F_j \end{aligned} \tag{9}$$

where K is symmetric and full. For three-dimensional displacements, ρ is $3n\times 1$ and K is $3n\times 3n$. Now we assign $\tilde{M}$ to be the coefficients of $\ddot{\rho}$ and N to be the coefficients of F, and we have in matrix form

$$\tilde{M}\ddot{\rho} + K\rho = Md^{\times}\dot{\omega} + NF \tag{10}$$

Φ for the cantilevered flex modes is normalized so that the modal masses are equal to one and

$$\Phi^{\mathrm{T}}M\Phi = E$$

$$\Phi^{\mathrm{T}}K\Phi = \Omega^2$$

Therefore, switching now to modal coordinates and making the above substitutions in Equation 10 we have

$$\begin{aligned} \tilde{M}\Phi\ddot{\eta} + K\Phi\eta &= Md^{\times}\dot{\omega} + NF \\ \Phi^{\mathrm{T}}\tilde{M}\Phi\ddot{\eta} + \Phi^{\mathrm{T}}K\Phi\eta &= \Phi^{\mathrm{T}}(Md^{\times}\dot{\omega} + NF) \\ \Phi^{\mathrm{T}}\tilde{M}\Phi\ddot{\eta} + \Omega^2\eta &= \Phi^{\mathrm{T}}(Md^{\times}\dot{\omega} + NF) \end{aligned} \tag{11}$$

This is comparable to the general form of a modal dynamics equation for a flexible system (including damping) (Gawronski 1998),

$$\ddot{\eta} + 2Z\Omega\dot{\eta} + \Omega^2\eta = Bu \tag{12}$$

where Z is the modal damping matrix and u are the nodal inputs, except that having $\tilde{M}$ will result in the combined model free frequencies being higher than the appendage cantilevered frequencies.

Next we move to development of the torque equation (3). First we write an intermediate step of the equation by substituting in the equation for $\ddot{d}$, neglecting only the nonlinear terms in $\dot{\rho}$ and $\dot{c}$:

$$\begin{aligned} T = I\dot{\omega} + \omega^{\times}I\omega \\ -\sum_{k=0}^{n} m_k d_k^{\times}(\omega^{\times}\omega^{\times}d_k - d_k^{\times}\dot{\omega} + \ddot{\rho}_k + \ddot{c}) \end{aligned} \tag{13}$$

The total inertia I_T is defined as

$$I_T = I_{\mathrm{core}} - \sum_{k-0}^{n} m_k d_k^{\times}d_k^{\times}$$

We gather terms which contribute to I_T, note that the sum of the terms involving $\ddot{c}$ is zero and ρ_0 is also zero, and convert to modal coordinates:

$$T = I_T\dot{\omega} + \omega^{\times}I_T\omega - \sum_{k=1}^{n} m_k d_k^{\times}\Phi\ddot{\eta} \tag{14}$$

The torque T is the sum of all external torques, including the torque onthe core T_c and any forces applied at the nodes.

$$T = T_c + \sum d_k^{\times}F_k \tag{15}$$

We can now write both the core and mass equations in matrix form with the terms containing $\dot{\omega}$ and $\ddot{\eta}$ on the left and the included modes 1-m listed explicitly. Let $I_M^j = \sum_k m_k d_k^{\times}\phi_k^j$, where ϕ_k^j is the 3×1 displacement vector for node k due to mode j. These terms indicate the contribution for each mode, which is a sum over the contributions from each node.

$$\begin{aligned} \begin{bmatrix} I_T & I_M^1 & \cdots & I_M^m \\ (I_M^1)^{\mathrm{T}} & & & \\ \vdots & & \Phi^{\mathrm{T}}\tilde{M}\Phi & \\ (I_M^m)^{\mathrm{T}} & & & \end{bmatrix} \begin{bmatrix} \dot{\omega} \\ \ddot{\eta}_1 \\ \vdots \\ \ddot{\eta}_m \end{bmatrix} \\ = \begin{bmatrix} -\omega^{\times}I_T\omega \\ -\Omega^2\eta \end{bmatrix} + \begin{bmatrix} T \\ \Phi^{\mathrm{T}}NF \end{bmatrix} \end{aligned} \tag{16}$$

Grouping the modal contributions into one matrix I_m and explicitly writing out the core and node inputs we have

$$\begin{aligned} \begin{bmatrix} I_T & I_m \\ I_m^{\mathrm{T}} & \Phi^{\mathrm{T}}\tilde{M}\Phi \end{bmatrix} \begin{bmatrix} \dot{\omega} \\ \dot{\eta} \end{bmatrix} = \\ \begin{bmatrix} (I_T\omega)^{\times} & 0 & 0 \\ 0 & -\Omega^2 & -2Z\Omega \end{bmatrix} \begin{bmatrix} \omega \\ \eta \\ \dot{\eta} \end{bmatrix} \\ + \begin{bmatrix} E_3 & d_0^{\times} & d_k^{\times} \\ 0 & \frac{\sum m_k\Phi^{\mathrm{T}}}{M} & \Phi^{\mathrm{T}} \end{bmatrix} \begin{bmatrix} T_c \\ F_c \\ NF_k \end{bmatrix} \end{aligned} \tag{17}$$

To obtain a state-space form from this equation, we will have to divide by the general inertia matrix on the left,

I_g. The output matrix C is composed of the submatrices ϕ for the output nodes of interest.

$$A = I_g \backslash \begin{bmatrix} (I_T\omega)^\times & 0 & 0 \\ 0 & -\Omega^2 & -2Z\Omega \end{bmatrix} \quad (18)$$

$$B = I_g \backslash \begin{bmatrix} E_3 & d_0^\times & d_k^\times \\ 0 & \frac{\sum m_k \Phi^T}{M} & \Phi^T \end{bmatrix} \quad (19)$$

$$C = \begin{bmatrix} 0\ \phi_{k_1,1-m}\ 0 \\ 0\ \phi_{k_2,1-m}\ 0 \end{bmatrix} \quad (20)$$

In addition, we have left in the $(I\omega)^\times$ nonlinear term for now, which will need to be linearized. If all rates are small, the term can be neglected. Otherwise, there are two common cases: first the presence of a large bias momentum (such as a momentum wheel), and second a steady body rate. In the case of bias momentum and small body rates, the bias drives the nonlinear term and the linearized version is simply

$$\omega^\times I\omega \approx -h_B^\times \omega$$

In the case of a steady rate ω_0, we linearize around the rate and drop terms of second order.

$$\begin{aligned} \omega^\times I\omega &= (\omega+\omega_0)^\times I(\omega+\omega_0) \\ &\approx (-(I\omega_0)^\times + \omega_0^\times I)\omega + \omega_0^\times I\omega_0 \end{aligned}$$

To complete our state-space representation we need to add states for the attitude kinematics. We consider three easily linearized cases, small Euler angles, small quaternion deviations, and perturbations from a rotating frame. Small 3-2-1 Euler angles can be integrated to first order directly from the body rates, giving

$$\dot{\theta} = \begin{bmatrix} 0 & E \end{bmatrix} \begin{bmatrix} \theta \\ \omega \end{bmatrix}$$

If the spacecraft is undergoing a steady rotation and we designate the nominal rate vector as ω_0, then the angular velocity is simplified with the small angle approximation as follows,

$$\omega \approx \dot{\theta} + (E - \theta^\times)\omega_0$$

Rearranging to solve for $\dot{\theta}$ we have

$$\dot{\theta} = \begin{bmatrix} -\omega_0^\times & E \end{bmatrix} \begin{bmatrix} \theta \\ \omega \end{bmatrix} - \omega_0$$

For small angle quaternions, the first component (q_s) is constant and the derivative reduces to one-half the body rates for the latter three terms (q_r),

$$\begin{bmatrix} \dot{q_s} \\ \dot{q_r} \end{bmatrix} = \begin{bmatrix} 0 & 0 & 0 \\ 0 & 0 & \frac{1}{2}E \end{bmatrix} \begin{bmatrix} q_s \\ q_r \\ \omega \end{bmatrix}$$

3. SIMPLE NON-COLLOCATED SYSTEMS

When a control vane or thruster is used at the tip of the solar sail for control the actuator is separated from the sensor by a flexible structure. If the bandwidth of the controller is much lower than the lowest flexible frequencies, as is the case with the solar sail control system discussed in this paper, this does not pose a problem. If the bandwidth approaches that of the bending modes then we have the classic noncollocated actuator/sensor problem. This section provides an introduction to the theory of control of systems with noncollocated actuators and sensors, an area that has been studied extensively in the context of large space structures control.

3.1. One-dimensional system

We begin our control analysis by compensating a simple 1 dimensional two-mass, one-spring system with a noncollocated sensor and actuator. The spring has a stiffness k and the system has damping c.

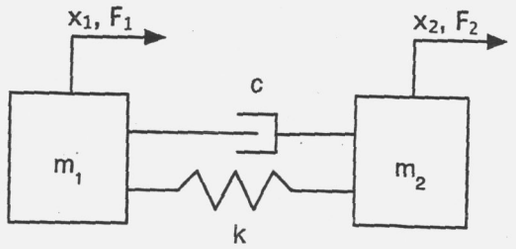

$$\begin{aligned} m_1\ddot{x}_1 + c(\dot{x}_1 - \dot{x}_2) + k(x_1 - x_2) &= F_1 \quad (21) \\ m_2\ddot{x}_2 + c(\dot{x}_2 - \dot{x}_1) + k(x_2 - x_1) &= F_2 \end{aligned}$$

In the frequency domain, neglecting damping for the moment, the system becomes

$$\begin{bmatrix} x_1 \\ x_2 \end{bmatrix} = \frac{\begin{bmatrix} s^2+w_2^2 & w_1^2 \\ w_2^2 & s^2+w_1^2 \end{bmatrix} \begin{bmatrix} F_1/m_1 \\ F_2/m_2 \end{bmatrix}}{s^2(s^2+(w_1^2+w_2^2))} \quad (22)$$

where $\omega_1^2 = k/m_1$ and $\omega_2^2 = k/m_2$. From this we see that for the collocated case F_2 to x_2, at low and high frequencies relative to the flex resonance the system acts like a rigid body, $1/s^2$. The lead from the zero(s) is cancelled by the lag from the pole(s) so that the phase after the flex frequencies remains 180°. For F_2 to x_1, however, at high frequencies the denominator approximates $1/s^4$, resulting in permanent phase lag. This is easily seen in the open loop response for both cases in Figure 4 on the next page.

The system properties are selected to give a natural frequency near the lowest sail mode. m_1 is 10 kg, m_2 is 1 kg, k is 0.3, c is 0.03, ω_n is 0.574 rad/s and Φ = [0.0953, −0.953].

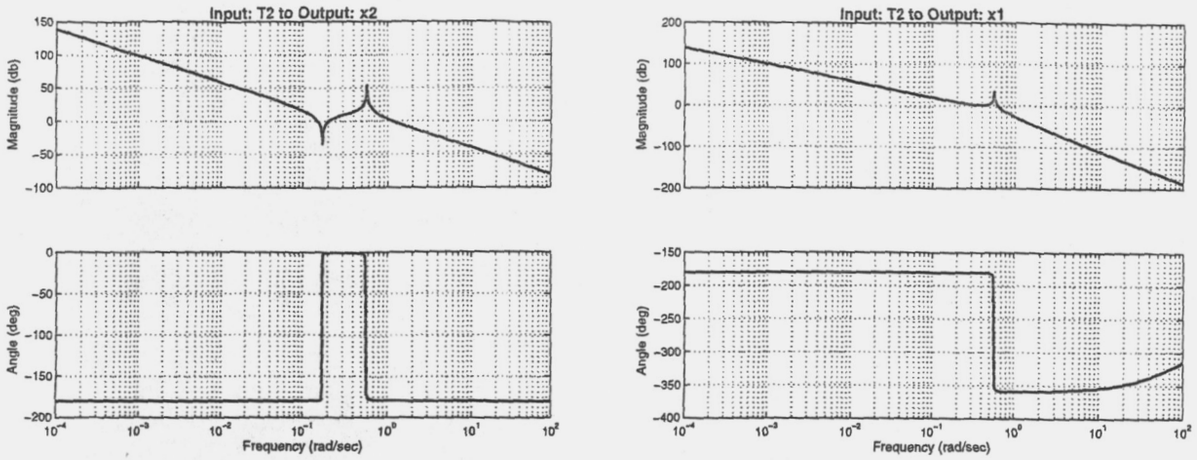

Figure 4. Open loop response for collocated (left) and non-collocated (right) actuation, 1D system

The state is $[x \;\; v]^{\mathrm{T}}$. The state space matrices are simple. First we define the stiffness, damping and mass matrices K, D and M,

$$K = \begin{bmatrix} k & -k \\ -k & k \end{bmatrix}$$

$$D = \begin{bmatrix} -c & c \\ c & -c \end{bmatrix}$$

$$M = \begin{bmatrix} m_1 & 0 \\ 0 & m_2 \end{bmatrix}$$

and then we can write out the state space.

$$A = \begin{bmatrix} 0 & E \\ -M^{-1}K & -M^{-1}D \end{bmatrix}$$

$$B = \begin{bmatrix} 0 \\ M^{-1} \end{bmatrix}$$

$$C = [\, E \;\; 0 \,]$$

We first apply a forward gain for the desired transient response, $K = 0.01$. The result is unstable as shown by the eigenvalues,

```
  -0.00165 +    0.57366i
  -0.00165 -    0.57366i
1.2661e-08 +   0.030193i
1.2661e-08 -   0.030193i
         0
```

We then add phase lead at the crossover frequency for the desired damping, with a maximum phase shift of 40°at $w_{max} = 1.0^{-2}$. This pushes the crossover frequency up, so we lower the gain to 0.001 and raise w_{max} to 2.0^{-2}, which gives a stable system with the eigenvalues

```
-0.0014114 +    0.57287i
-0.0014114 -    0.57287i
 -0.063411
 -0.021124
-0.0061566
          0
```

There is now a tradeoff between amount of phase lead and excitation of the flex mode. Figure 5 on the following page shows the open loop and step responses for phase leads of 40° and 65°.

Next we add a notch filter to reduce the gain seen by the flex mode. This should allow us to use the higher phase lead of 65° (i.e. more damping) with less excitation of the mode. We set the notch frequency equal to the resonant frequency (0.574 rad/s) with a gain reduction of 20 dB and a notch width of 0.1 rad/s. See Figure 6 on the next page, and note that the step response is lacking the small oscillation seen in Figure 5 on the following page.

Lastly, we need to add an integrator to drive the offset to zero. We will need this in the solar sail controller since the pointing during delta-V changes controls the thrust vector; we essentially want to limit the average pointing error over a maneuver within some tolerance. There is a trade between the time constant of the integrator and the forward gain; an infinitely high gain would result in a negligible offset, and correspondingly adding the integrator should allow for a higher gain. We will use a slow integrator of 3600 s, and add it in parallel with the lead compensator and filter. See Figure 7 on page 7 for the step response before and after the addition.

This same loop shaping procedure can be used with more complex systems such as the solar sail.

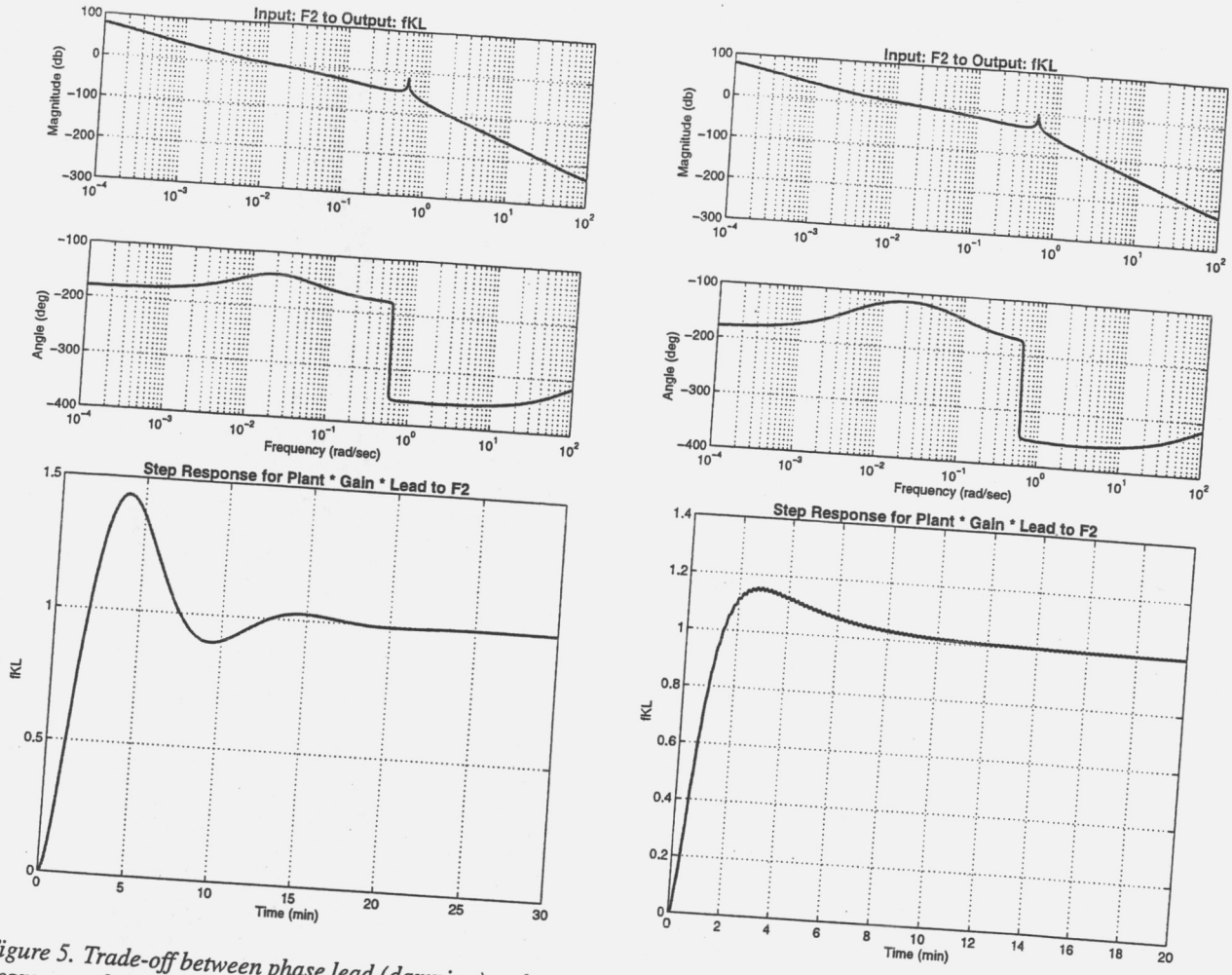

Figure 5. Trade-off between phase lead (damping) and mode excitation, for a phase lead of 40 degrees on the left and 65 degrees on the right, 1D system. Observe the small oscillation in the step response on the right.

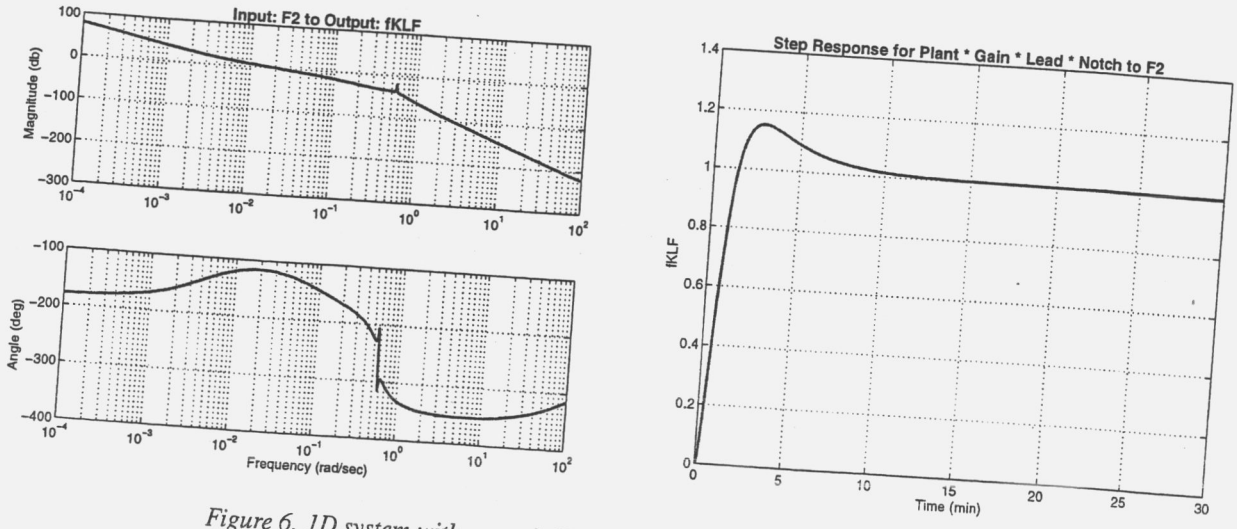

Figure 6. 1D system with a notch filter at the flex mode to smooth the response.

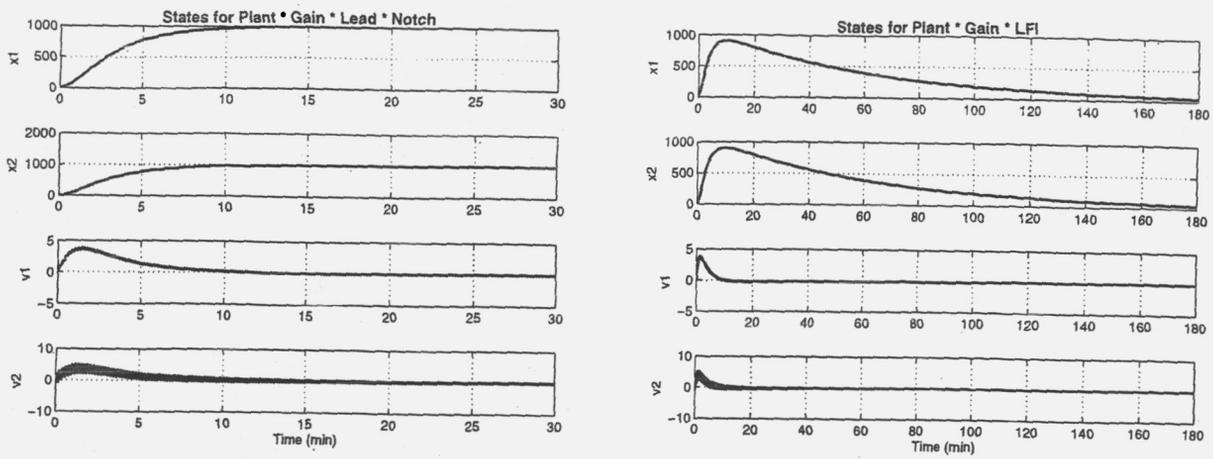

Figure 7. Step response of 1D system before and after integral is added.

3.2. Planar system

Now that we have established the response and control of the simplest flex system, we check our theoretical development for n flex nodes with a rotational planar system consisting of a core and two masses, having two flex frequencies. The core mass is 100 kg, m_1 is 2 kg and r_1 is 2 m, and m_2 is 1 kg and r_2 is 4 m, and the flex displacements are transverse to the node locations, as shown in Figure 8. For a spring stiffness of 0.5, the cantilevered natural frequencies are 0.38268 and 0.92388 rad/s. If the flex body is correctly linked to the core, we expect that the response to a force at r_2 will be 4 times the response to a unit torque on the core. We see in Figure 9 on the next page that we do get the collocated and noncollocated responses we expect. Note the upward shift of the flex frequencies from the cantilevered frequencies to the free frequencies.

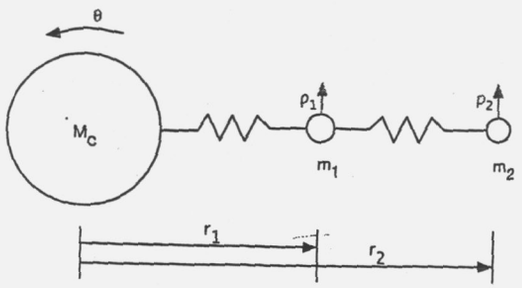

Figure 8. Simple rotational system

4. SOLAR SAIL ANALYSIS

In the case of the 80 m sail, the flex frequencies are relatively high compared to our desired control bandwidth ω_n of 0.002 rad/s(Wie et al. 2005), but also very close together, with the first 30 modes between 0.25 and 0.5 rad/s. The many overlapping poles and zeros may prevent us from seeing the clear noncollocated response as in the simple models.

First we check the open-loop sail plant as developed in Section 2, starting with the collocated response. Next

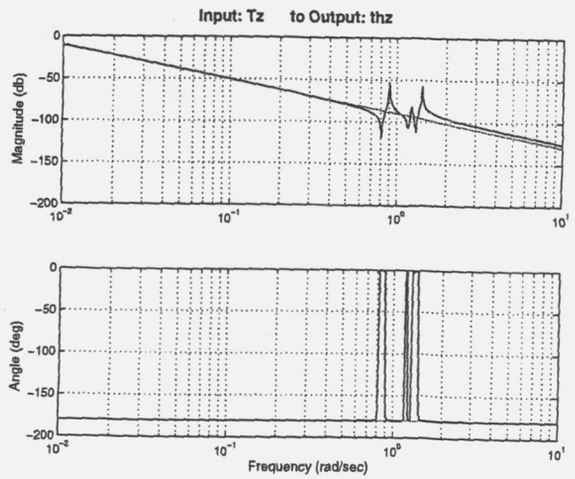

Figure 10. Sail plant response with modes 1-30

we consider our desired force input at a mast tip. We choose a node (50041) on the $+Y$ boom and consider forces in the $+X$ and $+Z$ directions, which will produce respectively $-T_z$ and $+T_x$. The inertia about the X axis is twice that of the other axes, and the boom tip is about 56 m from the core center. This is a complex system, and we do not see a simple noncollocated response in Figure 11 on the following page. We therefore also look at a node in the middle of a sail membrane (598). When including modes 1-4, we get a phase drop of 180° and a rigid body torque response (Figure 12 on page 9). Note the nodal output in the step response plots.

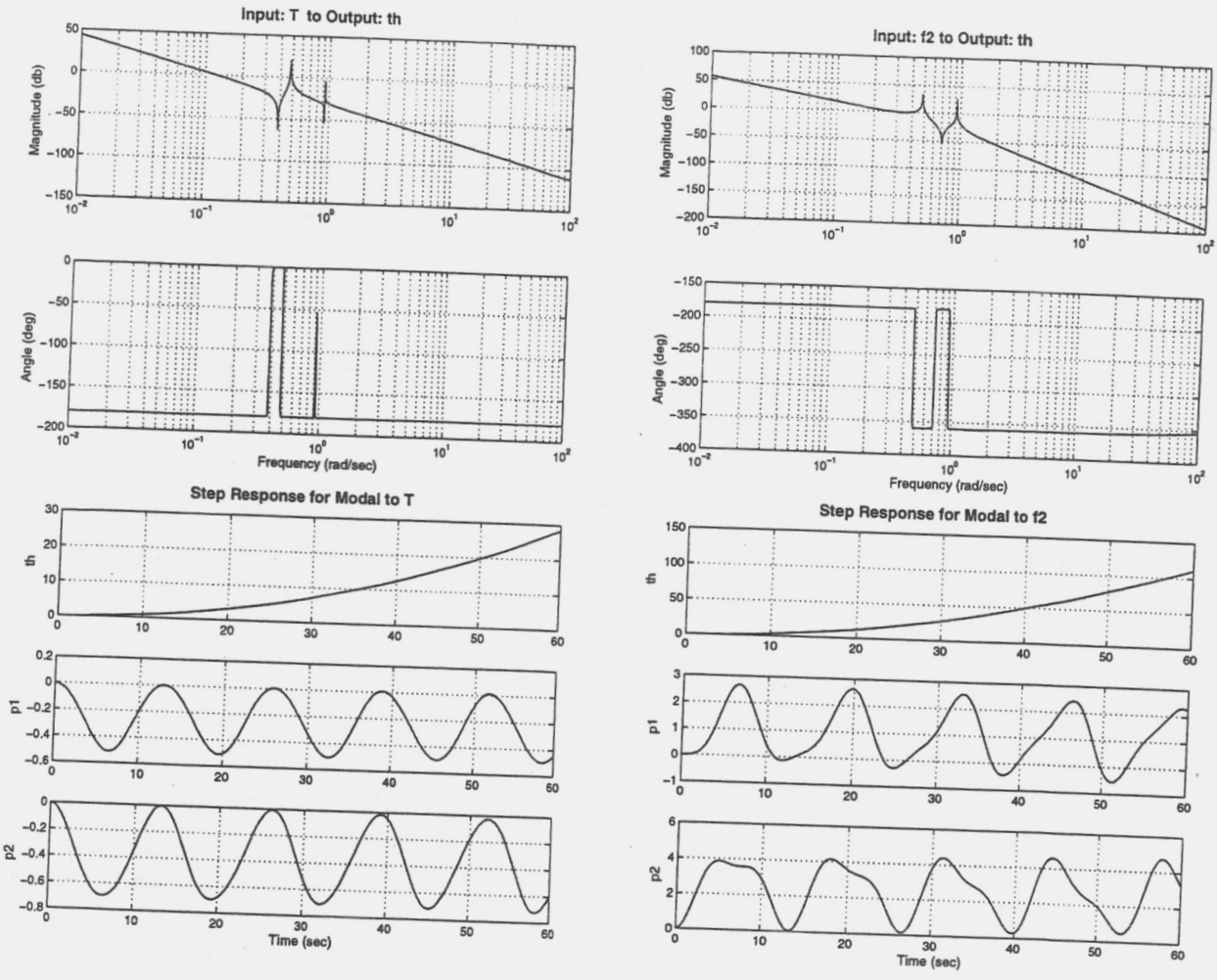

Figure 9. Response for a core with a 2 node flex body (planar system)

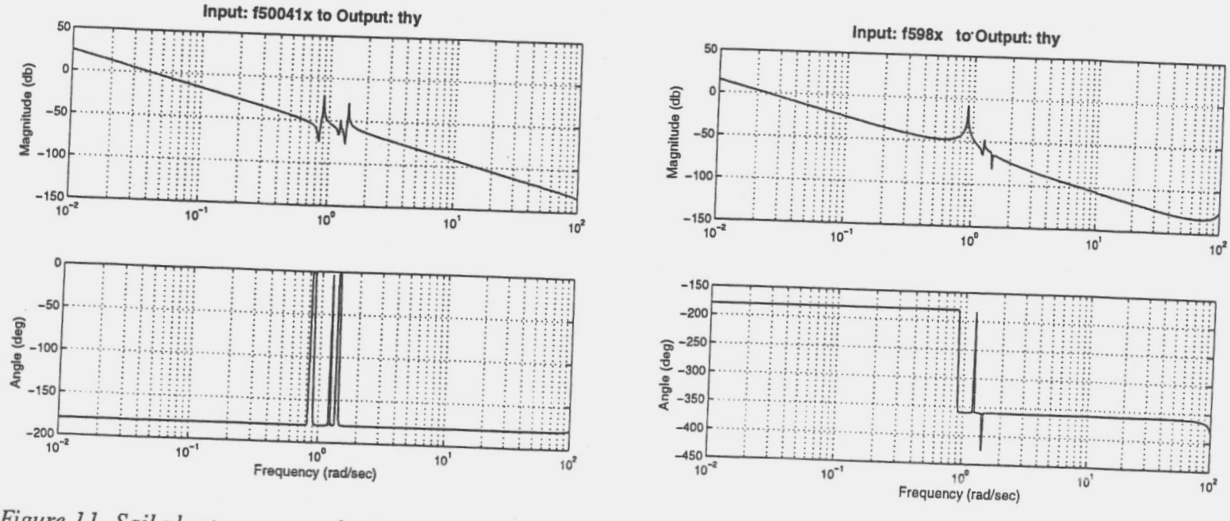

Figure 11. Sail plant response of sail to mast tip actuation (node 50041) and membrane actuation (node 598), including modes 1-30

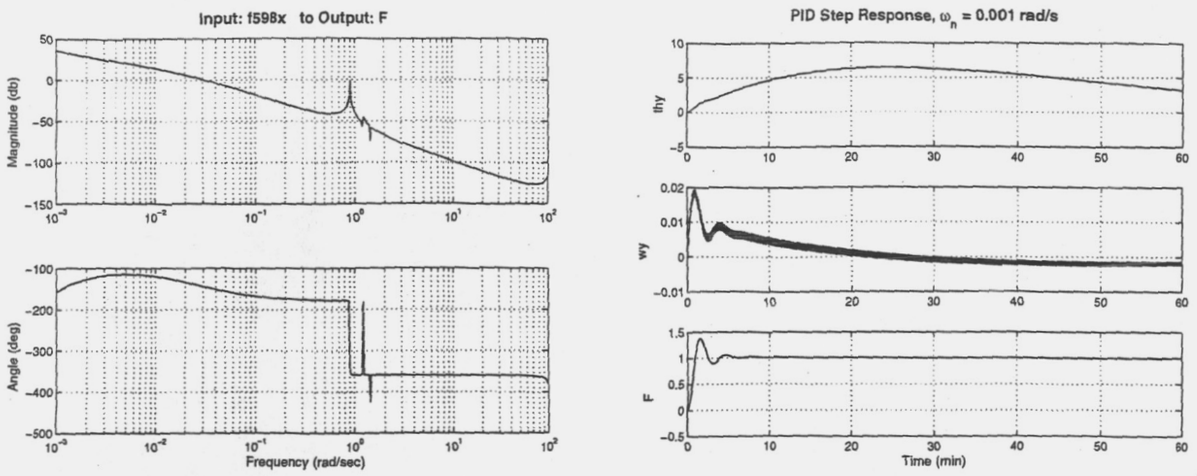

Figure 12. Membrane actuation (node 598) with PID controller, ω_n = 0.001 rad/s

We are interested in analyzing controllers at different bandwidths using our modal plant model. We first apply a PID controller, with modes 1-30 in the plant, and check the eigenvalues for stability. Both collocated actuation (core torques to core angles) and actuation at the mast tips are stable for all ω_n tried from 0.001 to 1 rad/s (with a damping ratio ζ of 0.8 and integrator time constant of 3600 s. However when the node in the membrane is considered, the system becomes unstable above 0.002 rad/s, so this provides an opportunity to try the loop shaping procedure outlined in Section 3 on page 4. Figure 12 shows the response with a PID controller at 0.001 rad/s for comparison. Note the crossover at about 0.02 rad/s.

Following the same procedure, we use a gain of 0.6, and a lead compensator with a maximum phase frequency of 0.12 rad/s and phase gain of 60°. Then we add a notch filter at the apparent frequency where the modes are clustered, about 1.5 rad/s, with a half-notch width of 1 rad/s and a gain drop of -30 dB. The frequency responses during this process and resulting stable step response are shown in Figure 13 on the following page. Note that we this compensator has a crossover frequency of about 0.1 rad/s.

Analyzing this sail configuration reminds us of an important fact, that the noncollocated response is irrelevant if the system is very stiff. In this case, the masts are very stiff relative to the sail membranes. Within the first 30 modes, only several have any boom involvement and those have very small displacement magnitudes. Although we might expect stability problems when performing actuation at the end of very long masts - here, 56 m - in fact there are none. However, actuating nodes on the membranes provides the expected response, both validating the analysis and indicating that if attitude sensing were for some reason placed on the membranes, or if in other configurations the supporting structure is equally flexible relative to the membrane modes, case must be taken in designing the control law.

ACKNOWLEDGEMENTS

The work described in this paper was funded in whole or in part by the In-Space Propulsion Technology Program, which is managed by NASA's Science Mission Directorate in Washington, D.C., and implemented by the In-Space Propulsion Technology Office at Marshall Space Flight Center in Huntsville, Alabama. The program objective is to develop in-space propulsion technologies that can enable or benefit near and mid-term NASA space science missions by significantly reducing cost, mass or travel times.

The authors would like to thank Dave Murphy and Tom Trautt of ATK Space Systems for their support in providing finite element models and feedback for this analysis.

REFERENCES

Gawronski, W. K. 1998, Dynamics and Control of Structures (Springer-Verlag)

Murphy, D. M., McEachen, M. E., Macy, B. D., & Gaspar, J. L. 2005, in Proceedings of 46th Structures, Structural Dynamics, and Materials Conference No. AIAA 2005-2126

Thomas, S., Paluszek, M., Wie, B., & Murphy, D. 2004, in Proceedings of AIAA Guidance, Navigation and Control Conference and Exhibit No. AIAA-2004-4890

Wie, B., Murphy, D., Paluszek, M., & Thomas, S. 2004, in Proceedings of AIAA Guidance, Navigation and Control Conference and Exhibit

Wie, B., Thomas, S., Paluszek, M., & Murphy, D. 2005, in Proceedings of AIAA Joint Propulsion Conference No. AIAA-2005-3928

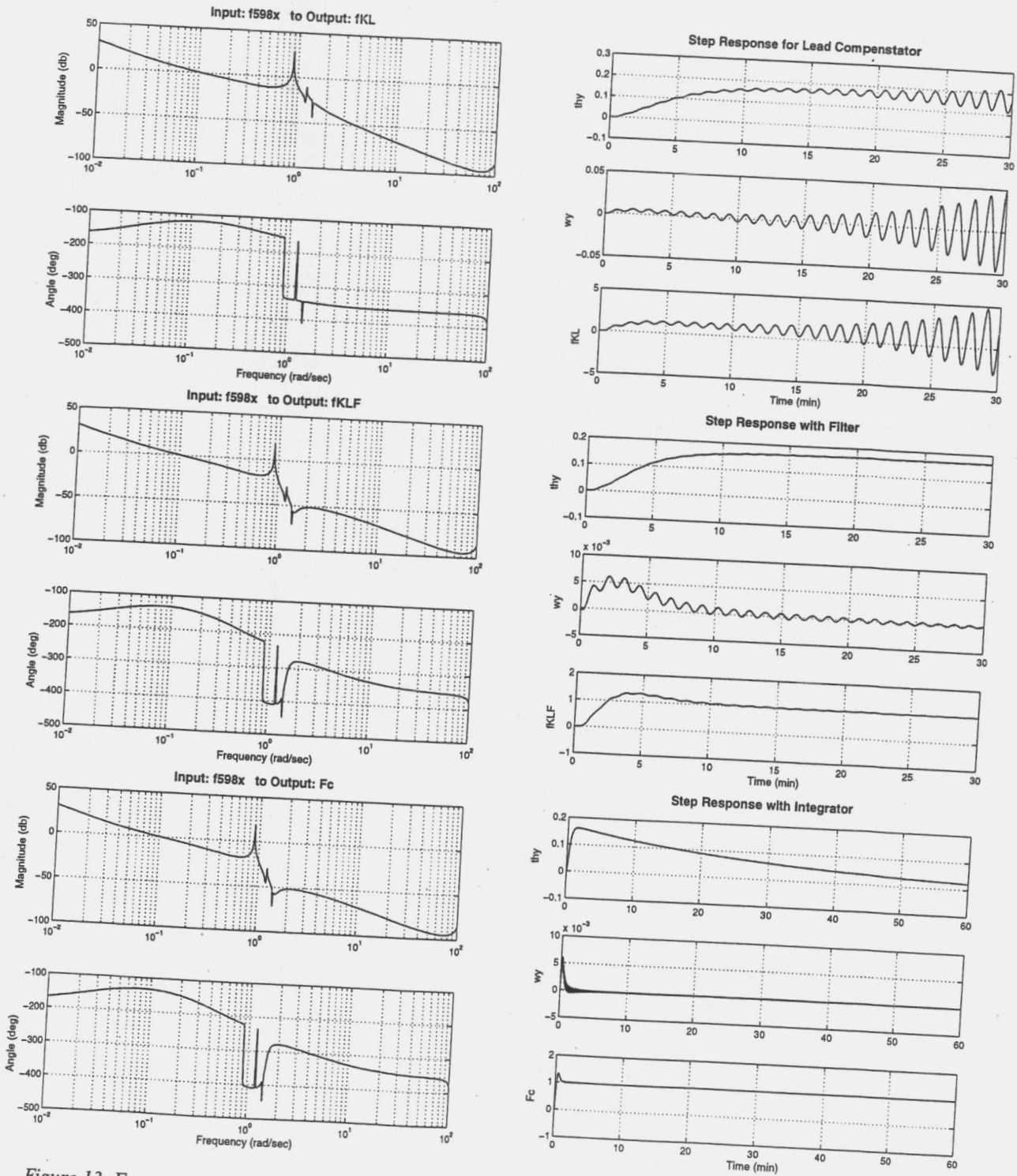

Figure 13. Frequency response of compensated sail, with gain and lead compensation, notch filter, and integrator.